Novel Graphene Structures: Substantial Capacity Enhancement in Lithium Batteries

Tereza M. Paronyan, Arjun K. Thapa, Andriy Sherihy, Jasek B. Jasinski, Samuel J. D. Jangam
University of Louisville, Louisville, KY, 40292, USA, *teparonyan@gmail.com*

ABSTRACT

Lithium-ion batteries (LIBs) as high energy- and power-density rechargeable batteries are in high demand for energy storage systems.

Novel 3D graphene structures were synthesized by CVD method using commercially available Ni and Cu powders. 3D pristine graphene structures were obtained which consist of up to 93% of incommensurately-stacked graphene. These structures exhibit over four times higher reversible capacity (up to 1540 mAh/g) than the theoretical capacity of graphite applied as an anode material in LIBs coin cells. These high capacities are stable throughout long-term cycling, and the retained capacity remains over 93% throughout hundred cycles by reaching up to 100% Coulombic efficiency for LiC_2 stoichiometry (1116 mAh/g capacity) [1]. We consider lithium intercalation model for multilayer graphene where capacity varies with N number of layers resulting $Li_{N+1}C_{2N}$ stoichiometry. LIBs based on incommensurate graphene anode promises new development of high capacity, cost-efficient and lightweight secondary batteries.

Keywords: graphene, Incommensurate, foam, high capacity, lithium battery

1. INTRODUCTION

Development of high capacity battery anode would significantly improve the advanced energy technologies and enhance the energy efficiency of many economic markets.

Graphite, consisting of commensurately-stacked infinite layers of graphene, is the commonly used anode material in Li-ion rechargeable batteries (LIBs) due to its high energy density and high power density, though with limited low capacity (372 mAh/g). The limited capacity is caused by low diffusion of lithium atoms into interplanar spaces. The strength of repulsive interactions that arise due to the orthogonality of interplanar π orbitals of sp^2 carbon excludes lithium diffusion between graphene layers, and in the result, the intercalation occurs at prismatic surfaces (arm-chair and zig-zag faces) only.

The absence of commensurately-stacking order within adjacent graphene layers outcomes in a weaker interplanar Van der Waals forces due to rotation or twisting. An increase in rotation angle between layers decreases

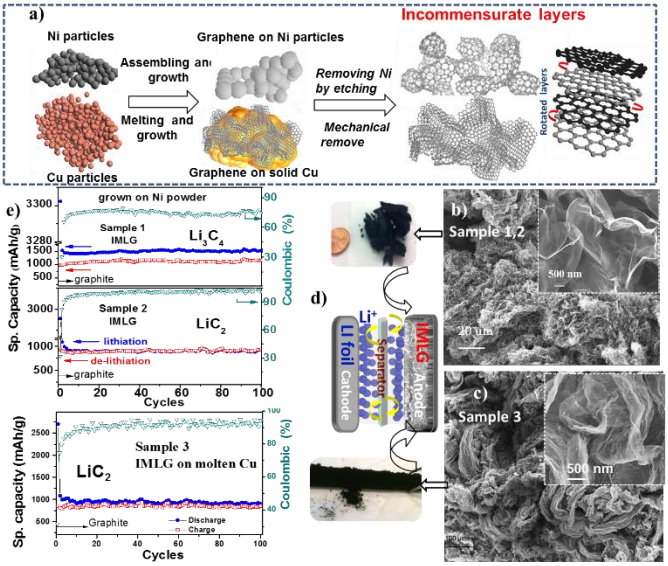

Figure 1: Illustration of IMLG preparation and testing in battery. a)-schematic illustration of the synthesis procedure. b)- SEM images with various magnifications of the Samples 1, 2 prepared on Ni powder and Sample 3 prepared on molten Cu (c). d)- battery cells construction and photographic images of the graphene powders e)- Charge-discharge results throughout 100 cycles of Samples 1,2 (upper graphs) and Sample 3(lower graph). Right axis shows Coulombic efficiencies of each sample.

interplanar interaction so that the incommensurate multilayers can be considered as a single graphene layer with modified electronic structure [2-4]. Thus, infinite layers of incommensurate graphene can be considered as a new type of "graphite-like" structure where the interplanar interaction forces are significantly weaker compared to graphite. In fact, the weakened interactions can enable easy penetration of small atoms between layers, and high current density can be collected due to superior electrical properties of graphene.

Here, we report of feasible fabrication techniques of incommensurately-stacked multilayer graphene (IMLG) structures and their exceptional Lithium intercalation capacities. IMLG networks containing over 85% incommensurateness demonstrate a reversible capacity of 1540 mAh/g (75 % coulombic efficiency) and 930 mAh/g (over 99% coulombic efficiency) corresponding Li_3C_4 and LiC_2 stoichiometry, respectively.

An effective capacity increase over six times compared to commercial graphite LIBs promises the feasibility of the rapid development of high-capacity, lightweight and cost-efficient rechargeable batteries based on IMLG anode.

2. RESULTS AND DISCUSSIONS

Micron-sized (3-50 μm) Nickel and Copper powders were used as a catalyst and 3D template to decompose the hydrocarbon source (methane) at high temperatures by CVD technique (schematically shown in Fig. 1a). Graphene grown on Ni particles at 1000-1090˚C were well-attached on Ni surface as a thin film (Fig. 2a).Graphene structures grown on Cu at 1070-1090˚C (Fig. 1c) were catalyst-free due to the melting of Cu (T_m=1085˚C).

High-purity (up 99% of Carbon) 3D porous multilayer (2-30 layers) graphene structures were acquired in the form of foam after removing the nickel from the template (Fig. 1b). Graphene foam consists of micron-sized curved thin sheets connected to each other without significant damage and agglomeration and which are separated from each other by micro-pores with micro-pores. The curvature of graphene sheets, presumably, originates from the catalyst shape since there is similarity in their morphology.

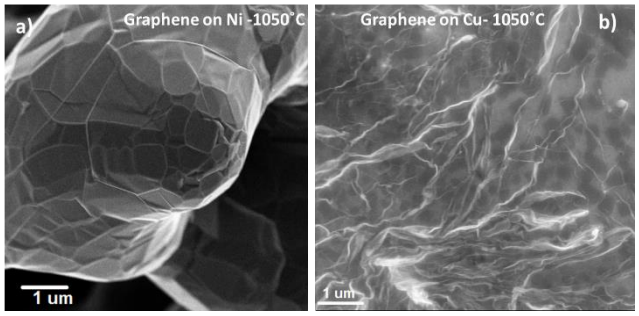

Figure 2: SEM images of graphene attached on Ni (a) and on Cu (b) particles grown at 1050˚C.

Raman spectrum provides the structural and electronic details of graphene, such as stacking order, the number of layers, quantity and nature of defects, and doping [5,6]. Raman spectra analysis revealed that Ni-free graphene foam contains incommensurately-stacking multilayers (IMLG) (Fig. 3a) with low defects (D band initiates from the defects). The incommensurate fraction of the foam was estimated by analyzing Raman 2D and G peaks which vary for the samples prepared at different conditions. Multilayer graphene 2D band either is single- or multi- Lorentzian fit discriminates between *commensurate* and *incommensurate* stacking. Also, we have found that the set of two values of Raman spectrum such as the full width of half maximum (FWHM) of the 2D band and I_{2D}/I_G (here, I_{2D} *and* I_G are the height of the 2D and G bands) can distinguish between *commensurate* and *incommensurate* stacking [1]. The higher is the ratio I_{2D}/I_G and a narrower 2D band are, the weaker the interplanar coupling is, thus closer resembling the spectrum of SLG (Sample 1 in Fig 3a). Several Raman maps were generated to estimate incommensurate

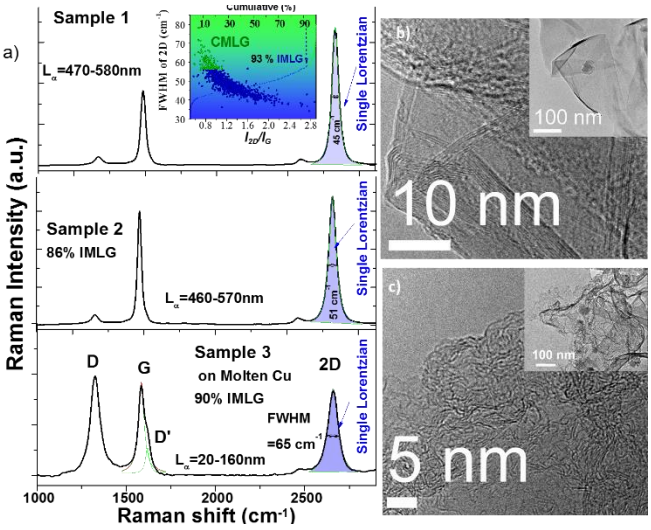

Figure 3: Structural analysis of graphene sheets. a)- averaged (over 300 spots) Raman spectra (λ=638nm) of Sample 1, 2, 3. Highlights show Lorentzian fit.
b)- HRTEM images of the Samples 1, 2 (prepared on Ni powder and Sample 3 prepared on molten Cu (c). (insets)- lower magnification images.

degree of each sample. Seven Ni-free samples (S1, S2, S4-S8) were analyzed for the battery tests which contain from 19% up to 93% incommensurateness.

Graphene grown on Cu powder consists 2-6 layers with increased boundary type of defects as revealed by Raman spectroscopy (Sample 3 in Fig. 3a) and high resolution transmission electron microscope (HRTEM) (Fig. 3c). An increased boundary defects are likely caused by wrinkling of the sheets (Fig.2 b) due to high growth temperatures (1050-1090˚C) caused by melting of Cu [7]. Graphene films grown at the lower growth temperatures (1000-1040˚C) were well attached on Cu surface and they perform a relatively lower Raman D band. Though, the yield of graphene sheets grown at higher temperatures was higher which allowed us to acquire enough amount of free-standing graphene powder for the battery tests.

L_a crystallite size and defect concentration were estimated by I_D/I_G (here, I_D is the height of D band) [8, 9]. L_a varies from 460 nm to 580 nm for Ni-free graphene sheets with estimated defect concentration of ~0.02% of carbon such as Sample 1, 2. L_a varies from 20 nm to 160 nm for graphene sheets grown on Cu with defect concentration of 0.09-0.74% of Carbon.

X-ray diffraction (XRD) pattern of Ni-free graphene foams show a sharp (002) peak at 2θ = 26.45° corresponding to the averaged *d* layer spacing of 3.36 Å accompanied small (004) peaks at 54.73°, (100) at 42.63° and (110) peak at 77.57° (inset-Fig. 5a). Last two peaks initiate from in-plane crystallinity of graphene while (002) and (004) peaks indicate interplanar parallel stacking. The diffraction peaks such as (101), (112), (113) *etc*. that originate due to ordering in *c*-axis are nearly absent indicating a very low concentration of commensurate stacking.

These graphene structures were applied as an anode materials in LIBs coin cells. The active material of graphene was weighed accurately in the range of 1 mg and it first was mixed with teflonized acetylene black (TAB-2) binder ratio (1:3 in mg).

Graphene material mixed binder was used as a working electrode and Li foil as a counter electrode separated from each other by glass fiber using 2032 Coin-type cell. 1 M solution of $LiPF_6$ was dissolved in a 1:2 ratio (by volume) of ethylene carbonate and dimethyl carbonate, and used as an electrolyte. The galvanostatic charge-discharge measurements were carried out using the "Arbin" instrument. Discharge and charge measurements were carried out at a voltage range of 3.0-0.005 V with different current densities of 0.1-5.0 A/g.

Electrochemical characterizations (EC) of the cells were tested throughout hundred cycles under 100 mAh/g currently density. The analyzing of seven Ni-free graphene samples revealed an increase of reversible capacity from 410 mAh/g up to 1540 mAh/g by a decrease of stacking commensurateness of the layers. Cu-free graphene anodes (Sample 3) perform similarity to some of the defect-free graphene (Sample 2) electrodes yet it performed more defects (Fig. 3a).

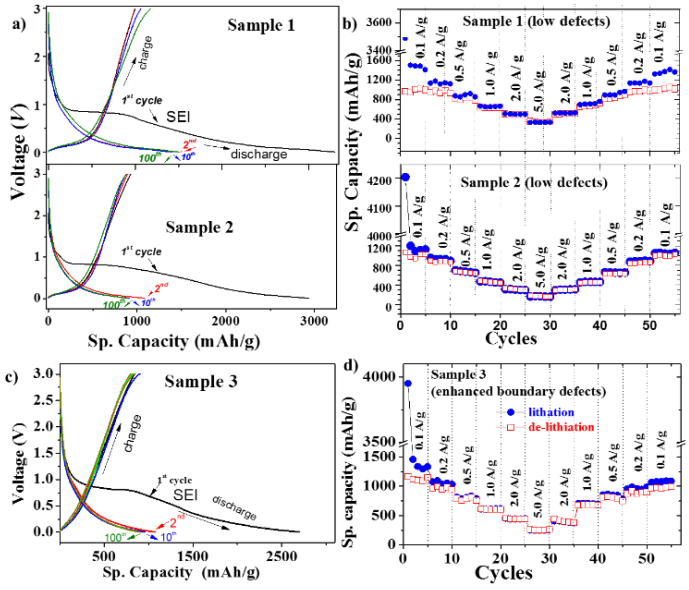

Figure 4: LiBs coin cells testing under 100mA/g current density. a)-voltage-discharge/charge profiles of a few cycles of Sample 1,2 and Sample 3 c). b)- *C*-rate testing under various current loads of Sample 1, 2 and Sample 3 d).

Voltage-charge/discharge measurements (Figs. 4a,b) show that initial discharge (lithiation) capacity profiles are different from the subsequent cycles caused by formation of a passivating film (referred to as the solid electrolyte interface-SEI). C-rate testing of high capacity cells (Fig 4b, d) demonstrated stability under higher current densities which make these cells feasible.

As the measured reversible capacities are considerably high, at that point we consider a lithium insertion model other

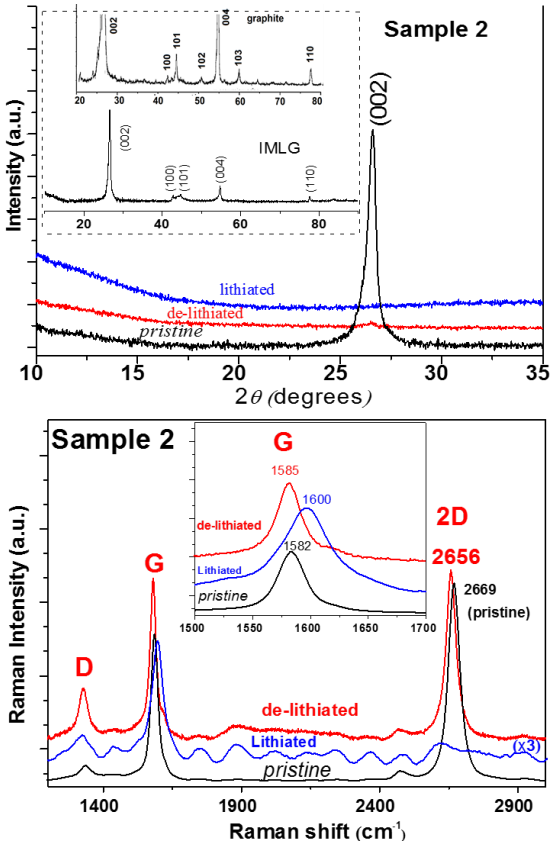

Figure 5: Structural analysis of IMLG anodes. a)-XRD pattern of (002) peak for lithaited and de-lithiated samples. (inset)-large spectrum of pristine IMLG and natural graphite. (b)-Raman analysis of the electrodes. The inset shows G band area.

than a model of LiC_2 proposed by Sato *et al* [10] which would explain any LiC_{2-x} ($0 \leq x \leq 2$) formation.

The absence of XRD (002) peak of the lithiated sample (Fig. 5a) and the significant shifts of Raman G and 2D bands (Fig. 5b) confirm that all galleries of incommensurately-interacted graphene sheets are fully occupied by lithium and they participate to charge transfer. Raman spectra of de-lithiated samples (Fig 5b) nearly returns back to the initial Raman spectrum of the pristine sample which confirms that no noticeable damage of graphene sheets occurred during long-term cycles.

Specific discharge capacity shows a nonlinear dependency of incommensurateness by reaching the maximum capacity of 1674 mAh/g that corresponds to Li_3C_4 (Fig. 6). This nonlinear dependency allows us to consider other factors such as the number of graphene layers and their interacted rotation angles may also affect the reversible capacity results. EC measurements of Sample 3 suggest that the increased boundary defects do not affect the LiBs capacity meanwhile an increase of commensurate stacking fraction of defect-free graphene significantly reduces the capacity of the cells (S8 in the graph of Fig 6). The reversible capacity reaches up to 100% Coulombic efficiency for LiC_2 stoichiometry (1116 mAh/g) as Samples 2 and Sample 3. Sample 1 performs up to 1540 mAh/g capacity with relatively lower (75%) Coulombic

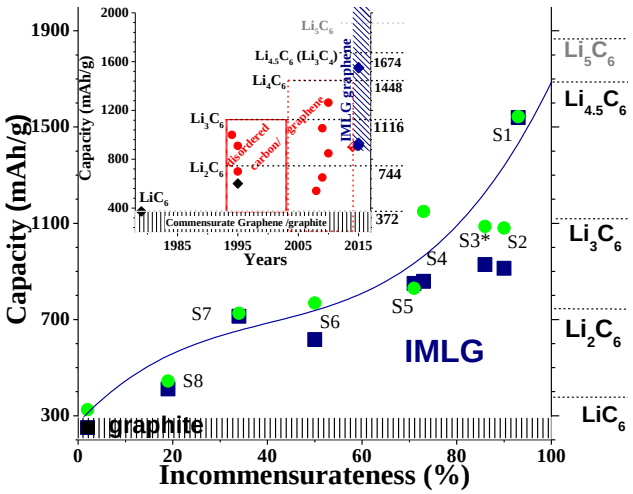

efficiency which is still stable throughout 100 cycles. The reversible capacity stabilized within the first 3-5 cycles, and after that charge-discharge retention remained over 95% throughout 100 cycles.

Figure 6: Discharge capacity dependency of graphene incommensurateness; solid circles represent second discharge capacities, solid squares represent discharge capacities at 100th cycle and half solid diagonal represent data obtained after long-term cycles. The inset shows significant data development of carbon based batteries; solid diagonals show capacities that were stable for long term cycling, circles shows capacities unstable for long-term cycling and high current loads.

In addition to structural and binding changes of lithiated graphene HRTEM observations (Fig. 7a,b) allowed us to propose a model where lithium atoms adsorb above and below each hexagon in the multilayer configuration. Then Li:C ratio would vary by N number of layers resulting $Li_{N+1}C_{2N}$ stoichiometry [1]. The capacity reaches maximum (1674 mAh/ g) when bilayer participates to charge transfer as Li_3C_4 while an infinite number of N would approach to LiC_2 (1116 mAh/g). This model would explain the capacity difference of the samples with nearly similar incommensurateness (Sample 1 with 93% IMLG and Sample 2 with 86 % IMLG).

In fact, incommensurate graphene layers provide fully intercalation of lithium atoms without any damage in graphene structure and that is capable of stable long-term charge-discharge cycling.

An effective capacity increase over six times, as compared to commercial graphite, promises the feasibility of the rapid development of lightweight, cost-efficient, high-capacity secondary batteries.

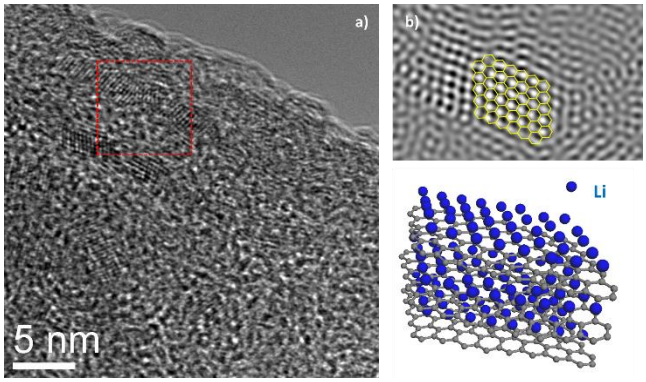

Figure 7: a)- (HRTEM) analysis of lithiated graphene sheets. b)- Fast Fourier Filtering (FFT) the masked area in a). graphene atomic structure is added on the aligned spots showing Li intercalation scheme. c)- Lithium intercalation model corresponding to $Li_{N+1}C_{2N}$ formula.

References

[1] Paronyan, T. M., Thapa A.K., Sherehiy A., Jasinski J., Dilip, J.S., *Incommensurate graphene foam as a high Capacity Lithium intercalation anode- Scientific Reports* **7**, srep39944, 2017. www.nature.com/articles/srep39944

[2] Li, G., *et al.* Observation of Van Hove singularities in twisted graphene layers. *Nature Physics* **6**, 109, 2010.

[3] Latil S., Menuier V., Henrard, L. Massless fermions in multilayer graphitic systems with misoriented layers: *Ab initio* calculations and experimental fingerprints. *Phys. Rev. B* **76,** 201402(1-4), 2007.

[4] Berashevich J. & Chakraborty, T. Interlayer repulsion and decoupling effects in stacked turbostratic graphene flakes. *Phys. Rev. B* **84**, 033403(1-4), 2011.

[5] Ferrari, A. C., Basko, D. M. Raman spectroscopy as a versatile tool for studying the properties of graphene. *Nature Nanotechnology* **8**, 235, 2013

[6] Malard, L. M., Pimenta, M. A., Dresselhaus, G., Dresselhaus, M.S.Raman spectroscopy in graphene. *Physics Reports* **473**, 51, 2009.

[7] Paronyan, T. M., Pigos, E. M., Chen, G., and Harutyunyan, A.R. The Formation of Ripples in Graphene as a Result of Interfacial Instabilities, *ACS NANO* **5**(12); pp. 9619, 2011.

[8] Cançado, L.G. *et al.* General equation for the determination of the crystallite size L_a of nanographite by Raman spectroscopy, *Applied Physics Letters* **88**, 163106(1), 2006.

[9] Cançado, L.G. *et al.* Quantifying Defects in Graphene via Raman Spectroscopy at Different Excitation Energies. *Nano Lett.* **11**, 3190, 2011.

[10] Sato, L., Noguchi, M., Demanchi, A., Oki, N., Endo, M. A mechanism of lithium storage in disordered carbons. *Science* **264**, 556, 1994.